# 1. SITE 958[1]

John V. Firth,[2] Peter Blum,[2] Sten Lindblom,[3] Klaus Michels,[4] William W. Sager,[5] and Amelie Winkler[6]

## INTRODUCTION

In December 1994, the *JOIDES Resolution* entered drydock in Falmouth, England, for routine maintenance and refurbishment, five years after its previous drydock. After drydock, the *Resolution* sailed south to Dakar, Senegal, for the port call that began Ocean Drilling Program (ODP) Leg 159. The date for arriving at Dakar was fixed, but if drydock work finished earlier than scheduled, or if the transit speed was faster than estimated, the ship might have had as much as one or two days of extra time before arriving in port. Because of this possibility, plans were made to take some cores at a site of opportunity along the transit, instead of letting the ship sit idle off the coast of Senegal. Because of the short-term planning for this contingency, the site had to be positioned out of any countries' territorial waters, in an area with little chance of encountering hydrocarbon hazards. In addition, the site could not be too far off the ship's track to Dakar, and should preferably be located along or near previously existing seismic survey lines. A potential site was located at the crossing point of *Glomar Challenger* Line 14 and *Vema* Line V-2908. It was close to previously existing ODP sites drilled during Leg 108 (Sites 657 and 658), in water depths intermediate between them (Fig. 1). Thus, it could provide complementary data to Leg 108 sites on paleoceanographic and paleoclimatic topics such as the history and nature of trade winds, surface water currents, and bottom water currents during the Neogene. Because only a short time might be available for drilling, only advanced hydraulic piston corer (APC) cores were planned to be taken.

Extra time was indeed available during the transit, so a short presite survey was made and 15 APC cores in two holes were taken at Site 958. No scientists were aboard the ship during the transit, and only 24 hours elapsed before reaching Dakar after finishing the site, so the cores were sectioned, run through the multisensor track, and stored in the core reefer. After Leg 159, they were shipped back to the Gulf Coast Repository in College Station, TX, where they were split, described, and analyzed on shore. An announcement was sent out in February 1995, describing the site, and inviting interested scientists to come and describe and sample the cores. Three scientists attended the core description and sampling meeting at ODP on June 13–16, 1995. Additional help in doing the basic core analysis came from scientists at ODP and Texas A&M University. Samples were taken for the meeting participants as well as for other shore-based scientists who could not make the description meeting. The purpose of the meeting was to provide the basic analysis that is routinely done on ship, in order to produce this site report, as well as to sample the cores for more detailed studies, which will be published in a future *Scientific Results* volume of the *Proceedings of the Ocean Drilling Program.*

### Authorship

The different sections of this site chapter were written by the following scientists (in alphabetical order, no seniority implied):

Introduction: Firth
Principal Results: Firth
Operations: Firth
Core Handling: Firth
Lithostratigraphy: Firth, Lindblom, Michels, Winkler
Biostratigraphy: Firth
Paleomagnetics: Sager
Carbonate Geochemistry: Lindblom
Physical Properties: Blum

## SITE SUMMARY

### Hole 958A

**Date occupied:** 29 December 1994, 1328 hr (UTC)

**Date departed:** 31 December 1994, 1625 hr (UTC)

**Time on hole:** ~51 hr

**Position:** 23°59.94′N, 20°00.05′W

**Water depth (sea-level; corrected m, echo-sounding):** 3728

**Bottom felt (rig floor, m, drill pipe):** 3795

**Distance between rig floor and sea level (m):** 10.5

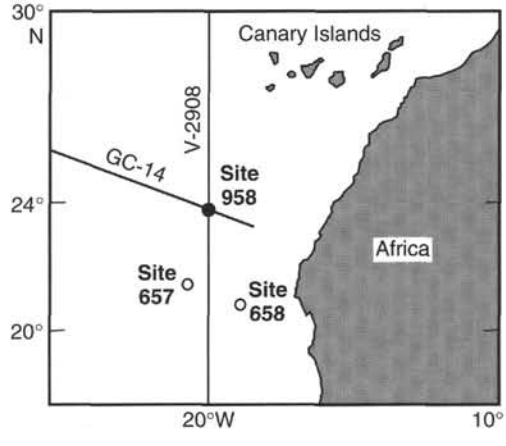


Figure 1. Map of eastern North Atlantic showing location of ODP Sites 958, 657, and 658, and seismic lines GC-14 and V–2908.

[1]Firth, J.V., et al., 1996, *Proc. ODP, Init. Repts.,* 159T: College Station, TX (Ocean Drilling Program).

[2]Ocean Drilling Program, 1000 Discovery Drive, Texas A&M University Research Park, College Station, TX 77845, U.S.A. Firth: John_Firth@odp.tamu.edu; Blum: Peter_Blum@odp.tamu.edu

[3]Department of Geology and Geochemistry, Stockholm University, S-10691 Stockholm, Sweden.

[4]Sonderforschungsbereich 313, Universitaet Kiel, Olshausenstrasse 40, Kiel, D-24118, Federal Republic of Germany.

[5]Department of Oceanography, Texas A&M University, College Station, TX 77843, U.S.A. sager@ocean.tamu.edu

[6]GEOMAR, Wischhofstrasse 1-3, Kiel, D-24148, Federal Republic of Germany.

**Total depth (rig floor, m):** 3928

**Penetration (m):** 133

**Number of cores:** 14

**Total length of cored section (m):** 133

**Total core recovered (m):** 130.99

**Core recovery (%):** 98.49%

**Oldest sediment cored:**
Depth (mbsf): 133
Nature: nannofossil ooze
Age: late Miocene

## Hole 958B

**Date occupied:** 31 December 1994, 1625 hr (UTC)

**Date departed:** 1 January 1995, 0230 hr (UTC)

**Time on hole:** ~10 hr

**Position:** 23°59.94′N, 20°00.05′W

**Water depth (sea-level; corrected m, echo-sounding):** 3728

**Bottom felt (rig floor, m, drill pipe):** 3788.8

**Distance between rig floor and sea level (m):** 10.5

**Total depth (rig floor, m):** 3797.5

**Penetration (m):** 8.7

**Number of cores:** 1

**Total length of cored section (m):** 8.7

**Total core recovered (m):** 8.19

**Core recovery (%):** 86.21

**Oldest sediment cored:**
Depth (mbsf): 8.7
Nature: nannofossil ooze
Age: Pleistocene

**Principal results:** Site 958 comprises 15 APC cores from two holes, penetrating to 133 mbsf with a total recovery of 139.18 m (98.22%). Comparison of lithologic, biostratigraphic, and physical properties data between the top two cores, 159-958A-1H and 159-958B-1H, indicates that there is little or no overlap between them; thus, there is about 7–10 m of sediment missing from above Core 159-958A-1H. Core 159-958B-1H established the mud line at 3778.3 mbsl. Because no exact measurement of the missing interval in Hole 958A can be made, all discussions of data are based on the top of Core 159-958A-1H as 0.0 mbsf.

The entire section is composed predominantly of nannofossil ooze, with a higher foraminifer content in the upper 30–40 m. Olive gray turbidites with higher foraminifer, quartz, biosilica, and organic matter content occur down to 29.55 mbsf in Hole 958A, and are the basis for distinguishing lithologic Subunit IA from the more nannofossil rich sediments of Subunit IB. Carbonate analyses also reflect the increasing carbonate content downhole. The upper part of Subunit IB (from about 29 to 45 mbsf) is characterized by low grain densities, bulk densities, and magnetic susceptibility. The sedimentation rate in this interval is also lower (about 1.3 cm/k.y.) than above or below, and a possible hiatus or condensed interval matches the discontinuity of physical properties at about 45 mbsf. A slightly higher content of quartz and biosilica between 30 and 45 mbsf may partly explain the lower densities. Light greenish gray color banding occurs throughout Subunit IB, but becomes more regular in band thickness and spacing below about Core 159-958A-10H (below 95 mbsf). The color bands have a higher clay content than the surrounding white nannofossil ooze. The bottom two cores, Cores 159-958A-13H and 14H, contain a few coarse-grained turbidites with higher foraminifer and quartz content.

Calcareous nannofossil biostratigraphy indicates that Site 958 contains a nearly complete sequence from Quaternary to upper Miocene (<6.5 Ma). Zone NN17 and Subzone NN16b were not recognized, and may be absent because of a hiatus, or may be condensed. Sedimentation rates based on nannofossil datums vary from 2.3 cm/k.y., between 0 and 20 mbsf, to 1.3 cm/k.y., from 20 to 55 mbsf, and 2.8 cm/k.y., from 55 to 130 mbsf.

Initial sampling for discrete paleomagnetic measurements was not detailed enough to determine a magnetostratigraphy for the site; however, high magnetic intensities correlated with the higher magnetic susceptibilities, and weakly magnetized samples correlated to the low magnetic susceptibility interval in the middle of the section.

## OPERATIONS

After drydock in Falmouth, England, the *JOIDES Resolution* departed at 1000 hr (local), 23 December 1994, and was underway for port call in Dakar, Senegal, to pick up scientists for the beginning of Leg 159. At 1200 hr, 29 December, a short pre-site survey was started for Site 958 (Figs. 2, 3), with crossing lines over the crossing point of *Glomar Challenger* Line 14 and *Vema* Line V-2908. A Datasonics beacon was dropped at 1328 hr, 29 December. After returning to the site, an APC/XCB bottom-hole assembly (BHA) was rigged up and

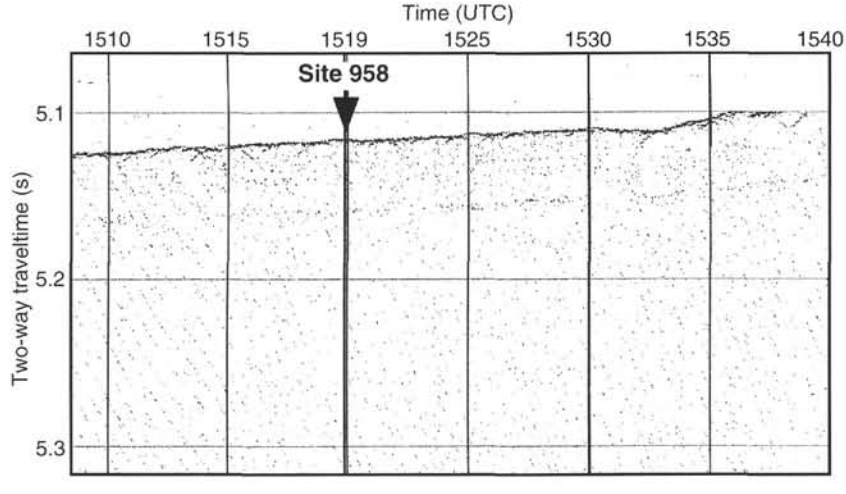


Figure 2. 3.5-kHz profile across Site 958.

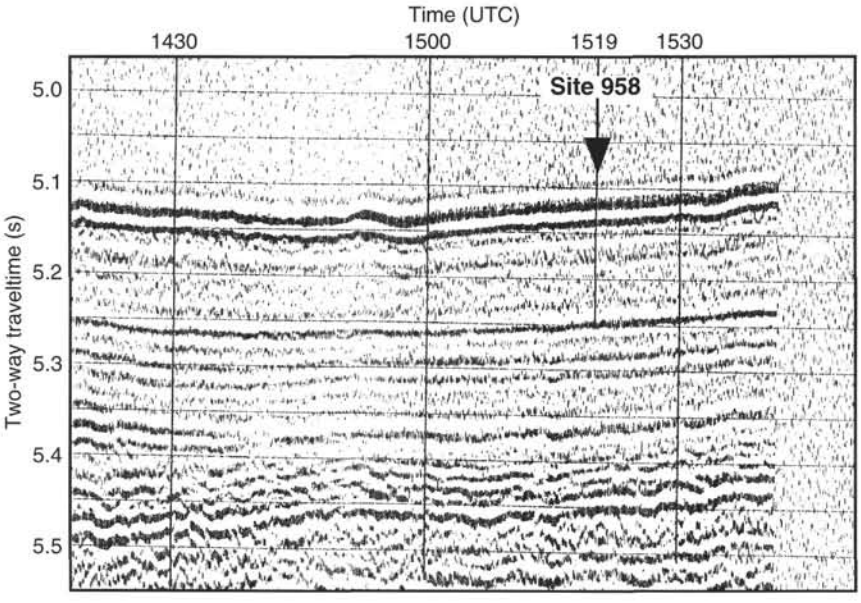


Figure 3. Seismic profile across Site 958.

lowered to the seafloor. A delay occurred when the APC core barrel did not land successfully in the BHA and had to be pulled out. The BHA had apparently been lowered into the sediment, resulting in some bent pipe, and thus stopped the core barrel from landing inside. After pulling up and rigging up a second BHA, the APC core barrel was successfully landed and Core 159-958A-1H was taken at 0210 hr, 31 December. Cores 159-958A-1H through 14H advanced to 133.08 meters below seafloor (mbsf), with 99.65% recovery (Table 1). Hole 958A is located at 23°59.94′N, 20°00.05′W. Because Core 159-958A-1H had full recovery, a second hole was spudded to establish the mud line. Core 159-958B-1H penetrated 8.7 m, and established the mud line at 3788.8 meters below rig floor (3778.3 meters below seafloor). After this core was taken, the drill pipe was pulled up, ending Site 958. The ship was under way at 0318 hr, 1 January 1995, for Dakar.

## CORE HANDLING PROCEDURES

When cores arrived on deck, they were cut into 1.5-m sections and their ends were capped. Whole round sections of 5 to 10 cm in length were taken from Section 5 of Cores 159-958A-1H, 2H, 3H, 4H, 5H, 8H, 11H, and 14H for interstitial pore water (IW) analyses. The IW samples were sealed and stored with the cores until shipment after Leg 159. Each section was then run through the multisensor track (MST) to log natural gamma, gamma-ray attenuation porosity evaluator (GRAPE) density, *P*-wave velocity, and magnetic susceptibility. Only Section 159-958A-8H-1 was split, run through the cryogenic magnetometer, and demagnetized to 20 mT. Routine headspace samples were taken for monitoring hydrocarbon safety, with only trace amounts of methane and ethane found. Numbering of site, holes, cores, and samples follows standard ODP procedures. All cores were sent to the Gulf Coast Repository (GCR) at Texas A&M University for splitting, description, photography, and analyses. When the cores arrived at the GCR, the IW samples were squeezed and the pore waters sealed and stored. These pore waters are available for sampling.

## LITHOSTRATIGRAPHY

### Sediment Core Description and Classification

Sediment core description followed the standard shipboard procedure, using the VCD program to produce barrel sheets. Symbols for sedimentary lithologies, structures, disturbance, and samples follow

**Table 1. Coring summary for Site 958.**

| Core | Date (December 1994) | Time (UTC) | Depth (mbsf) | Length cored (m) | Length recovered (m) | Recovery (%) |
|---|---|---|---|---|---|---|
| 159-958A- | | | | | | |
| 1H | 31 | 0235 | 0–9.5 | 9.5 | 9.86 | 103.79 |
| 2H | 31 | 0340 | 9.5–19 | 9.5 | 9.7 | 102.11 |
| 3H | 31 | 0435 | 19–28.5 | 9.5 | 9.01 | 94.84 |
| 4H | 31 | 0535 | 28.5–38 | 9.5 | 9.92 | 104.42 |
| 5H | 31 | 0635 | 38–47.5 | 9.5 | 9.09 | 95.68 |
| 6H | 31 | 0735 | 47.5–57 | 9.5 | 9.14 | 96.21 |
| 7H | 31 | 0840 | 57–66.5 | 9.5 | 8.95 | 94.21 |
| 8H | 31 | 0940 | 66.5–76 | 9.5 | 9.43 | 99.26 |
| 9H | 31 | 1045 | 76–85.5 | 9.5 | 9.39 | 98.84 |
| 10H | 31 | 1145 | 85.5–95 | 9.5 | 9.51 | 100.11 |
| 11H | 31 | 1245 | 95–104.5 | 9.5 | 9.7 | 102.11 |
| 12H | 31 | 1335 | 104.5–114 | 9.5 | 9.35 | 98.42 |
| 13H | 31 | 1430 | 114–123.5 | 9.5 | 8.35 | 87.89 |
| 14H | 31 | 1543 | 123.5–133 | 9.5 | 9.59 | 100.95 |
| Total cored: | | | | 133 | 130.99 | 98.49 |
| 159-958B- | | | | | | |
| 1H | 31 | 1810 | 0 | 8.7 | 8.19 | 86.21 |
| Total cored: | | | | 8.7 | 8.19 | 86.21 |

the standard ODP scheme as found in, for example, Ruddiman, Sarnthein, Baldauf, et al. (1988; Leg 108) and the *Initial Reports* for Leg 159 (this volume). The sediment classification scheme of ODP Leg 108 (Ruddiman, Sarnthein, Baldauf, et al., 1988) was used for Site 958. Color was determined using Munsell Soil Color Charts (Munsell Soil Color Charts, 1971).

Site 958 Holes A and B consist of mainly nannofossil ooze with a higher foraminifer content in the upper 30–40 m. Coring disturbance is minor except for the top sections of Cores 159-958A-1H, 7H, and the bottom section of Core 159-958A-10H. Sediments are generally slightly bioturbated. The section is assigned to one sedimentary unit with two subunits that are distinguished mainly on foraminifer content and the occurrence of turbiditic sediments (Fig. 4).

#### *Unit I*

Top: 0.0 mbsf, top of Core 159-958B-1H
Base: 133.01 mbsf, base of Core 159-958A-14H

*Subunit IA*

Top: 0.0 mbsf, top of Core 159-958B-1H
Base: 29.55 mbsf, interval 159-958A-4H-1, 105 cm

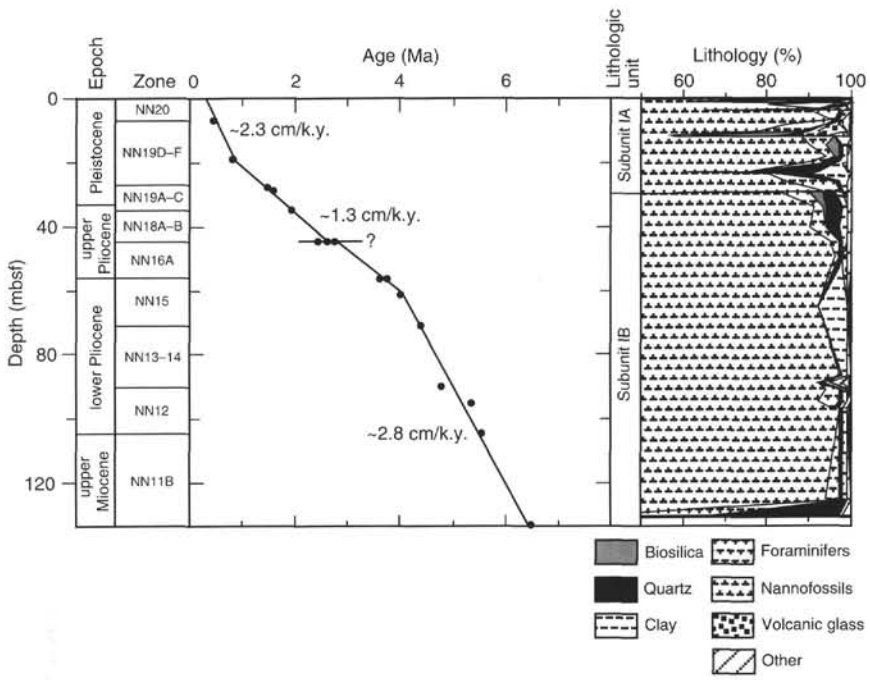


Figure 4. Summary figure of lithologic components (based on smear-slide analysis), sedimentary units, calcareous nannofossil zonation, age, and sedimentation rate curve.

Core 159-958A-1H recovered a full core liner with 9.5 m of sediment; thus, the mud line was not adequately established in this core. After Hole 958A was cored, Core 159-958B-1H was taken a few meters away from Hole 958A to establish the mud line at 3778.3 mbsl. Core 159-958B-1H recovered 8.7 m of sediment. The top four sections of Core 159-958B-1H consist of pink to brownish gray foraminiferal nannofossil ooze, which does not occur in Core 958A-1H. Only small flecks of this pinkish brown sediment are seen in the top of Section 159-958A-1H-1. This suggests that at least 6 m of the sediment column are missing from above Core 159-958A-1H. Nannofossil biostratigraphy (see "Biostratigraphy" section, this chapter) also indicates that at least the upper 3.75 m of Core 159-958B-1H were not recovered in Hole 958A. Therefore, the top of lithologic Unit I is placed at the top of Core 159-958B-1H rather than Core 159-958A-1H.

Subunit IA consists in the upper 5 m of slightly bioturbated, pink to brownish gray foraminifer nannofossil ooze with intervals exhibiting slight variations in color. From 5 to 29.55 mbsf, this subunit consists of mainly white to light gray, slightly bioturbated foraminifer-bearing nannofossil ooze. Occurring within this sequence are several dark olive gray fining-upward sequences, up to 50 cm thick, which display sharp basal contacts, and consist of more silty to sandy quartz-rich lower parts overlain by a finer grained greenish gray diatom-bearing nannofossil ooze. The upper contacts appear gradational and often contain a more or less distinct band of light greenish gray. Below Section 159-958A-2H-2, bands of greenish gray and gray frequently occur. The base of Subunit IA is placed at the base of the lowermost foraminifer-rich olive gray silty layer in Section 159-958A-4H-1.

*Subunit IB*

Top: 29.55 mbsf, Section 159-958A-4H-1, 105 cm
Base: 133.01 mbsf, Section 159-958A-14H-CC, 24 cm

Subunit IB consists mainly of mottled white, slightly bioturbated nannofossil ooze. Light greenish gray color banding of irregular thickness and distribution occurs from Cores 159-958A-4H through 9H. From Cores 159-958A-10H down to the bottom of the section, distinct light gray layering occurs, with a more regular thickness of 10–20 cm below Core 159-958A-10H, and the interval spacing between layers is between 50 and 100 cm. The distinct light gray layers are finer grained and more clayey than the white intervals. Bioturbation is more apparent where there are color changes between white and light gray. Small black specks and spots are dispersed throughout the sediments. Thin, black manganese banding occurs occasionally throughout the section.

Two thin (3–10 cm) dark gray coarser grained, fining upward layers occur in Cores 159-958A-13H and 14H. Soft sediment deformation (characterized by folded or broken layering) occurs in Section 159-958A-4H-1, and also in Sections 159-958A-13H-6 and 13H-7. Occasional elongate pyritized burrows are found in this subunit. In Section 159-958A-4H-5, there are two large (2–3 cm) clasts of finely granular pyrite, mixed with nannofossil ooze.

### Interpretation

The overall sequence at Site 958 is characterized by hemipelagic sedimentation. The olive gray fining upward layers in the upper four cores of Hole 958A, and in Cores 159-958A-13H and 14H, are similar to those found in Sites 950, 951, and 952 from the Madeira Abyssal Plain, which are interpreted as organic-rich turbidites.

## BIOSTRATIGRAPHY

Calcareous nannofossils were analyzed using smear slides. The zonation of Martini and Müller (1986) modified by Young (1991) was used. The datums used for calculation of sedimentation rates were correlated to the geochronologic time scale following Weaver, Schmincke, Firth, et al. (in press). Relative abundances and preservation were recorded according to the scale used in Srivastava, Arthur, Clement, et al. (1987).

Calcareous nannofossil biostratigraphy indicates that Site 958 contains a mostly complete sequence from Quaternary to upper Miocene. Nannofossils are abundant and well preserved throughout. Nannofossil datums from this site are listed in Table 2. Zones are shown in Figure 4.

**Table 2. Calcareous nannofossil datums and zones from Holes 958A and 958B.**

| Core, section, interval (cm) | Depth (mbsf) | Age (Ma) | Genus | Species | Datum | Zone |
|---|---|---|---|---|---|---|
| 159-958B- | | | | | | |
| 1H-3, 74 | 3.74 | 0.26 | *Emiliania* | *huxleyi* | LO | Base NN21 |
| 159-958A- | | | | | | |
| 1H-5, 111 | 7.11 | 0.46 | *Pseudoemiliania* | *lacunosa* | HO | Top NN19F |
| 2H-CC, 31 | 19.19 | 0.83 | *Reticulofenestra* | *asanoi* | HO | |
| 3H-CC, 19 | 28.01 | 1.47 | *Helicosphaera* | *sellii* | HO | Top NN19C |
| 4H-1, 106 | 29.07 | 1.60 | *Calcidiscus* | *macintyrei* | HO | Top NN19B |
| 4H-5, 89 | 34.90 | 1.95 | *Discoaster* | *brouweri* | HO | Top NN18B |
| 5H-3, 150 | 42.50 | | *Discoaster* | *triradiatus* | HO Acme | Top NN18A |
| 5H-5, 67 | 44.67 | 2.44 | *Discoaster* | *pentaradiatus* | HO | Top NN17 |
| 5H-5, 67 | 44.67 | 2.61 | *Discoaster* | *surculus* | HO | Top NN16B |
| 5H-5, 67 | 44.67 | 2.76 | *Discoaster* | *tamalis* | HO | Top NN16A |
| 6H-CC, 26 | 56.63 | 3.77 | *Reticulofenestra* | *pseudoumbilica* | HO | Top NN15 |
| 6H-CC, 26 | 56.63 | 3.62 | *Sphenolithus* | *abies* | HO | |
| 7H-3, 150 | 61.50 | 4.01 | *Discoaster* | *tamalis* | LO | |
| 8H-3, 150 | 71.00 | 4.39 | *Amaurolithus* | *tricorniculatus* | HO | Top NN14 |
| 10H-3, 150 | 90.00 | 5.04 | *Ceratolithus* | *rugosus* | LO | Top NN12 |
| 10H-CC, 18 | 95.01 | 5.34 | *Triquetrorhabdulus* | *rugosus* | HO | |
| 11H-CC, 22 | 104.69 | 5.56 | *Discoaster* | *quinqueramus* | HO | Top NN11B |
| 14H-CC, 26 | 133.08 | 6.50 | *Amaurolithus* | *amplificus* | LO | |
| 14H-CC, 26 | 133.08 | | *Amaurolithus* | *delicatus* | LO | Base NN11B |

### Hole 958A

The top of Hole 958A (Sample 159-958A-1H-1, 0 cm) does not contain either *Emiliania huxleyi* or *Pseudoemiliania lacunosa,* and is assigned to Zone NN20. Almost all zones and subzones down to Subzone NN11b occur in this hole. Zone NN17 and Subzone NN16b were not observed, either because they have very narrow age ranges and may have been missed in sampling, or because there is a short hiatus between Subzone NN16a and NN18a (Fig. 4) between 44.67 and 42.5 mbsf (Samples 159-958A-5H-5, 67 cm, and 5H-3, 150 cm). Some other subzones were not differentiated because the markers are rare or have sporadic occurrences. Further shore-based work may refine the subzones in this section.

### Hole 958B

The lowest occurrence of *Emiliania huxleyi* is in Sample 159-958B-1H-3, 74 cm. The base of Core 159-958B-1H lies above the highest occurrence of *P. lacunosa,* and is assigned to Zone NN20. Because the top of Hole 958A is in Zone NN20, and because of lithologic differences between Cores 159-958A-1H and 159-958B-1H (see "Lithostratigraphy" section, this chapter), the most reasonable explanation of missing Zone NN21 in Core 159-958A-1H is that the top few meters of sediment were not recovered in this core. Because no nannofossil datums are common between Cores 159-958A-1H and 159-958B-1H, no exact correlation can be made between them. However, the base of *E. huxleyi* at 3.74 mbsf in Hole 958B indicates that at least this much section is missing from the top of Hole 958A.

## SEDIMENTATION RATES

Nannofossil datums and depths used for calculation of sedimentation rates are found in Table 2. The top 19 m of Hole 958A has an approximate sedimentation rate of 2.3 cm/k.y. (Fig. 4). Extrapolating the sedimentation rate curve to the top of Hole 958A indicates an age of about 0.25 Ma at 0 mbsf. This supports the conclusion (above) that at least 4 m of sediment, representing at least Zone NN21 (0.27 m.y.), was not recovered from the top of Hole 958A, but was recovered in Hole 958B. Between 19 and about 61 mbsf, the sedimentation rate is approximately 1.3 cm/k.y. At about 44.6 mbsf, three nannofossil datums coincide, and two short zones are missing between 44.6 and 42.5 mbsf. A short hiatus may be represented in this interval, or the sample spacing may not be close enough to differentiate the missing zones. Between about 61 and 133 mbsf, the sedimentation rate is approximately 2.8 cm/k.y.

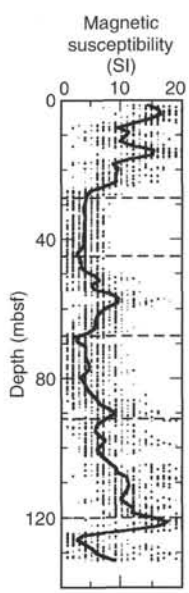


Figure 5. Volume magnetic susceptibility vs. depth from Hole 958A.

## PALEOMAGNETICS

Shipboard paleomagnetic examination of Site 958 cores departed somewhat from the usual shipboard routine. As usual, magnetic susceptibility measurements were made on whole core sections when the cores were run through the MST track on board ship. Because the cores were not split on board ship, this precluded the usual measurements made with the pass-through cryogenic magnetometer. However, later, on shore, 11 pilot samples were collected in 7-cm$^3$ plastic cubes for analysis of magnetic properties.

### Magnetic Susceptibility

Figure 5 shows volume magnetic susceptibility measurements made with the Bartington MS-2 susceptibility meter on the MST.

**Table 3. Paleomagnetic sample data.**

| Sample | Depth (mbsf) | NRM (mA/M) | Incl. (degree) | N | AF steps (mT) | MAD (degree) | MDF (mT) | SIRM (mA/m) |
|---|---|---|---|---|---|---|---|---|
| 159-958A- | | | | | | | | |
| 1H-4, 14–16 | 4.64 | 6.90 | 38.6 | 7 | 15–60 | 1.1 | 28.7 | 1188.40 |
| 2H-4, 96–98 | 14.96 | 5.35 | –45.1 | 5 | 25–50 | 1.3 | 28.1 | 2052.64 |
| 2H-6, 126–128 | 18.26 | 7.61 | –41.5 | 7 | 15–60 | 0.9 | 28.0 | 1665.31 |
| 3H-4, 47–49 | 23.97 | 4.13 | –38.0 | 7 | 10–50 | 2.7 | 21.5 | 1102.66 |
| 4H-6, 106–108 | 37.06 | 0.09 | 61.8 | 2 | 5–10 | 2.2 | 3.2 | 31.27 |
| 5H-2, 83–85 | 40.33 | 0.07 | –20.1 | 5 | 10–30 | 6.9 | 10.0 | 47.11 |
| 6H-4, 88–90 | 52.88 | 6.90 | 52.1 | 7 | 10–50 | 1.2 | 25.7 | 847.85 |
| 8H-4, 74–76 | 71.74 | 12.89 | 69.9 | 7 | 10–50 | 0.9 | 8.5 | 1270.27 |
| 10H-5, 55–57 | 92.05 | 8.57 | 54.1 | 5 | 15–40 | 4.5 | 5.0 | 2255.79 |
| 12H-4, 83–85 | 109.83 | 7.18 | 60.9 | 7 | 10–50 | 1.5 | 8.1 | 1050.64 |
| 159-958B- | | | | | | | | |
| 1H-3, 67–69 | 3.67 | 11.31 | 34.0 | 7 | 10–60 | 1.0 | 28.9 | 2608.61 |

Notes: NRM = natural remanent magnetization; Incl. = inclination of mean remanent magnetization determined using a linear least-squares fit tied to origin (see Kirschvink, 1980); N = number of measurements used to determine mean magnetization vector; AF steps = alternating field demagnetization steps used for calculation of mean magnetization vector; MAD = maximum angle of deflection, an error estimate (see Kirschvink, 1980); MDF = mean destructive field (i.e., AF demagnetization at which magnetization is reduced by half); SIRM = saturation isothermal remanent magnetization (at 1000 mT).

These data are raw and have not been corrected for the difference between the calibration volume and core volume. Nevertheless, they accurately reflect relative variations in susceptibility within the sediment column. A broad trend is notable with higher values (10 to 20 SI) at the top and bottom of the section and low values (2 to 5 SI) between about 28 to 49 mbsf and 67 and 85 mbsf. Furthermore, evidence of shorter wavelength variations, with amplitudes of about 10 SI, are seen within the sections having higher susceptibilities. The longer wavelength variations probably represent epochal (over millions of years) changes in sedimentary source, whereas the shorter wavelength variations are likely climate fluctuations with periods on the order of tens of thousands of years, perhaps owing to glacial/interglacial cycles. A similar record was obtained from ODP Sites 721 and 722, located at nearly the same latitude to the east of Africa (deMenocal et al., 1991).

## Paleomagnetic Properties

Magnetic measurements for the 11 discrete samples (Table 3) were made with a CTF cryogenic magnetometer. After the natural remanent magnetization (NRM) was measured, each sample was demagnetized using the alternating field (AF) technique at steps of 5, 10, 15, 20, 25, and 30 mT, for all samples, and a subset of 35, 40, 50, 60, 70, 80, and 100 mT, depending on the sample magnetization strength and the demagnetization performance (Fig. 6). After demagnetization, three samples had stepwise isothermal remanent magnetizations (IRM) applied using a pulse magnetizer, up to fields of 1000 to 1200 mT (Fig. 7). The remainder of samples were treated with an applied field of 1200 mT, to yield a saturation remanent magnetization (SIRM).

Magnetization directions from the AF demagnetization experiments were plotted on orthogonal-vector (Zijderveld) plots. Mean magnetization directions were calculated for each sample using measurements from a univectorial decay portion of the plot and fitting a linear least-squares line anchored to the origin (Kirschvink, 1980). Mean paleoinclinations are given in Table 3.

NRM intensities ranged over two and a half orders of magnitude, from 0.07 mA/m to 12.89 mA/m. Most samples are strongly magnetic compared to average deep-sea sediments. This suggests that the sediments contain a component derived from erosion of continental rocks with abundant magnetic grains. The weakly magnetized sediments are from Cores 159-958A-4H and 5H, coincident with the magnetic susceptibility low between 28 and 48 mbsf.

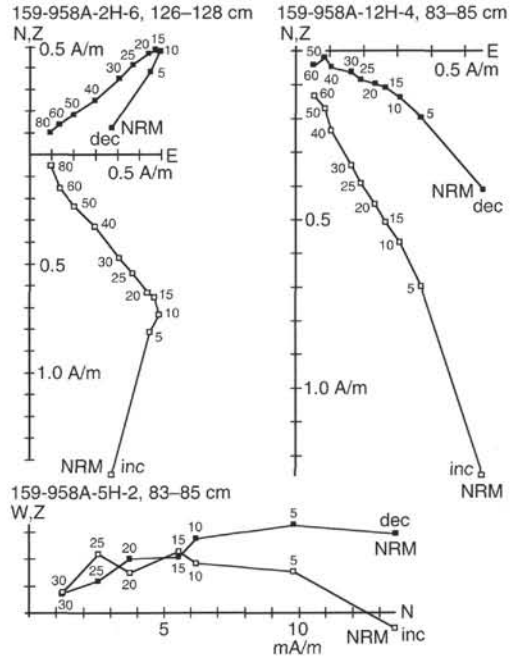


Figure 6. Orthogonal vector (Zijderveld) plots of vector endpoints from AF demagnetization of three samples from Hole 958A. At top are two strongly magnetic samples from the top and bottom of the section. Below is a weakly magnetic sample from the middle section of the hole. Note that the bottom plot scales are marked in mA/m, whereas the top plots are in A/m. Open symbols = the projection of the inclination on a vertical plane; filled symbols = the projection of the declination on a horizontal plane.

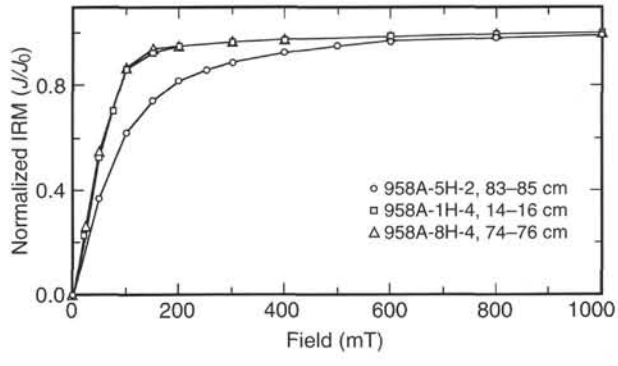


Figure 7. IRM acquisition curves for three samples from Hole 958A. Measurements have been normalized by dividing with the SIRM value. Samples 159-958A-1H-4, 14–16 cm, and 159-958A-8H-4, 74–76 cm, from the top and bottom of the section, give virtually indistinguishable IRM acquisition curves. The other sample is from the weakly magnetic section of sediments at middle depths in the hole.

The orthogonal vector plots indicate that all but one sample displayed a stable characteristic remanence direction that was isolated with variable amounts of AF demagnetization. Strongly magnetic samples from the top and bottom of the section displayed isovectorial decay throughout much of the demagnetization (Fig. 6). Reversed magnetization samples (e.g., Sample 159-958A-2H-6, 126–128 cm) typically showed an overprint opposite in direction to the characteristic remanence, implying that the overprint is a present-day normal polarity artifact. Overprints on reversed polarity samples typically took greater demagnetization (15 to 20 mT) to remove than did over-

prints from normal polarity samples (5 to 10 mT; Fig. 6). This is likely a result of a small difference between the direction of the overprint and the characteristic remanence direction.

The two weakly magnetic samples did not give directions that were as consistent as the other samples because their magnetic moments were close to the sensitivity level of the magnetometer. Nevertheless, their directions were sufficiently consistent (e.g., Sample 159-958A-5H-2, 83–85 cm) to determine polarity and calculate a mean direction (Table 3).

Mean destructive field (MDF) values ranged from 3.2 to 28.7 mT (Table 3). Lower values were obtained from the weakly magnetic samples and those from the bottom of the section. MDF values for samples from the upper three cores were uniformly high. This distribution implies subtle differences in the magnetic grains in these sections. The upper section appears to contain grains that are more magnetically stable, with less propensity to acquire an overprint. Below about 25 mbsf, more of the magnetic grains are unstable. Sediments in the middle of the section do not have a high concentration of magnetic grains and hence their magnetizations are weak. In contrast, sediments from the bottom of the section have higher NRM values, indicating a higher concentration of magnetic grains, but these magnetizations are removed by low AF fields, indicating many of the grains have low-coercivity magnetic moments. Figure 7 shows that samples from the top and bottom sections have very similar IRM acquisition curves, implying their magnetic minerals are similar. These samples become saturated in fields of 150 mT or less, which is typical of titanomagnetite. The one weakly magnetic sample for which an IRM acquisition curve was measured (Fig. 7) acquired most of its SIRM in low applied fields; however, it required 600 mT to come within 3% of the SIRM. This implies that some of the magnetic grains in this sample have high magnetic coercivities. From the existing data, it cannot be determined whether the high-coercivity grains are only evident in the weaker samples owing to being overwhelmed by more magnetic lower-coercivity grains in the other samples (i.e., they are ubiquitous, but masked in most places) or whether they are not found in the other samples.

Figure 8 shows that SIRM values plotted vs. depth roughly mimic the variation in magnetic susceptibility with high values in the top and bottom of the section. The lowest values were given by the two weakly magnetic samples from Cores 159-958A-4H and 5H. This similarity in pattern indicates that the concentration of magnetic grains dictates both the susceptibility and SIRM values. One difference between the susceptibility and SIRM curves is that the samples from Cores 159-958A-6H and 8H, at depths of 52.8 and 71.7 mbsf, gave relatively high SIRM values, whereas the susceptibilities from these depths are about the same on average as those which yielded weakly magnetic samples. One possible explanation is that the magnetic grains are somewhat different, but another plausible explanation is that the two samples from Cores 159-958A-6H and 8H were inadvertently taken from small layers with higher susceptibility.

### Magnetic Polarity

From the small number of samples measured, it is impossible to construct a magnetic stratigraphy; however, the results allow some observations about magnetic polarities and the fidelity of the sediments as magnetic recorders. Only three of 11 samples have reversed polarity. In particular, all of the samples below 50 mbsf have normal polarity. This is unexpected because this section spans approximately 4 to 7 Ma, a period of abundant magnetic reversals (Cande and Kent, 1992). Although the number of samples is small, so this observation may not be statistically significant, it suggests that a drill-string overprint may not be completely removed from these samples. Another observation in favor of this hypothesis is that the characteristic magnetizations have steeper than expected inclinations. The geocentric axial dipole field inclination for Site 958 is approximately 38°, and as much as 15° to 20° variation from this mean is not unusual; however, the four deepest samples have inclinations of 52.1° to 69.9° (Table 3).

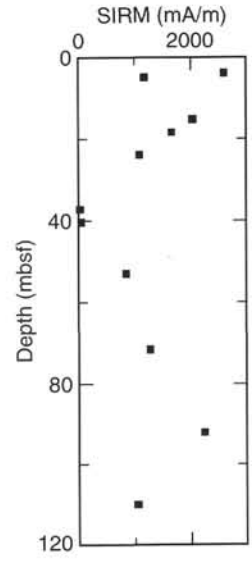


Figure 8. SIRM vs. depth for samples from Hole 958A.

Above 50 mbsf, the samples are roughly half normal and half reversed. The reversed polarity samples from Core 159-958A-2H imply that the Matuyama reversed chronozone is at that level. Given that the biostratigraphy indicates an age of about 0.7 to 1.0 Ma for this section (see "Biostratigraphy" section, this chapter), this must be the upper part of the Matuyama (Cande and Kent, 1992). The other reversed sample, at a depth of about 40.3 mbsf, is probably from the bottom of the Matuyama chronozone.

## CARBONATE GEOCHEMISTRY

Carbonate analyses were performed according to the methods explained in Ruddiman, Sarnthein, Baldauf, et al. (1988). The entire sequence sampled for carbonate analyses consists of nannofossil ooze with minor differences in other constituents. At distinct levels, olive green turbidites occur, varying in thickness from a few centimeters to 0.3 m. Samples for carbonate analysis were taken from almost every section. Results are shown in Table 4 and Figure 9. Carbonate content varies between 28% and 94%. The lower values from the upper part of the sequence correspond to dark olive green turbidites, presumably with a higher organic carbon content. There is a general trend of increasing carbonate content with depth. Further analyses of mineral content (by XRD) and organic carbon and nitrogen will be reported later.

## PHYSICAL PROPERTIES

### Depth Scale and Completeness of Cored Section

As discussed in the "Operations" section (this chapter), the first core of Hole 958A had full recovery, so Core 159-958B-1H was taken to determine the mud line. Based on lithologic and biostratigraphic evidence, there is at least 6 m of sediment missing from above Core 159-958A-1H. However, the continuous records of gamma-ray attenuation density and magnetic susceptibility, as well as porosity and gravimetric density at Site 958 indicate that there is no overlap between the two cores (Fig. 10). It is impossible to say exactly how much material is missing from above Core 159-958A-1H, and which is the actual mbsf reference for Hole 958A data. We chose to illus-

**Table 4. Carbonate analyses, Site 958.**

| Sample | Depth (mbsf) | Carbonate (%) |
|---|---|---|
| 159-958A- | | |
| 1H-2, 55–56 | 2.05 | 62.79 |
| 1H-3, 68–69 | 3.68 | 28.07 |
| 1H-4, 104–105 | 5.54 | 62.98 |
| 1H-5, 113–114 | 7.13 | 88.96 |
| 1H-6, 65–66 | 8.15 | 85.75 |
| 1H-7, 45–46 | 9.45 | 69.94 |
| 2H-1, 71–72 | 10.21 | 74.12 |
| 2H-2, 91–92 | 11.91 | 42.42 |
| 2H-3, 84–85 | 13.34 | 72.08 |
| 2H-4, 78–79 | 14.78 | 45.68 |
| 2H-5, 91–92 | 16.41 | 72.10 |
| 2H-6, 96–97 | 17.96 | 86.21 |
| 2H-7, 7–8 | 18.77 | 83.79 |
| 3H-1, 64–65 | 19.64 | 33.67 |
| 3H-2, 94–95 | 21.44 | 72.84 |
| 3H-3, 94–95 | 22.94 | 31.66 |
| 3H-4, 85–86 | 24.35 | 39.11 |
| 3H-5, 77–78 | 25.77 | 62.62 |
| 3H-CC, 8–9 | 27.90 | 82.16 |
| 4H-1, 88–89 | 29.38 | 49.06 |
| 4H-2, 106–107 | 31.06 | 75.01 |
| 4H-3, 106–107 | 32.56 | 57.97 |
| 4H-4, 68–69 | 33.68 | 62.83 |
| 4H-6, 55–56 | 36.55 | 62.04 |
| 4H-7, 54–55 | 38.04 | 80.46 |
| 5H-1, 123–124 | 39.23 | 79.08 |
| 5H-2, 78–79 | 40.28 | 74.68 |
| 5H-3, 126–127 | 42.26 | 63.15 |
| 5H-4, 105–106 | 43.55 | 85.44 |
| 5H-5, 107–108 | 45.07 | 80.60 |
| 5H-6, 42–43 | 45.92 | 78.97 |
| 6H-2, 42–43 | 49.42 | 51.28 |
| 6H-3, 80–81 | 51.30 | 62.71 |
| 6H-4, 105–106 | 53.05 | 78.41 |
| 6H-5, 102–103 | 54.52 | 83.08 |
| 6H-6, 83–84 | 55.83 | 75.44 |
| 7H-1, 80–81 | 57.80 | 56.53 |
| 7H-2, 45–46 | 58.95 | 82.82 |
| 7H-3, 52–53 | 60.58 | 80.14 |
| 7H-4, 97–98 | 62.47 | 84.15 |
| 7H-5, 145–146 | 64.45 | 54.54 |
| 7H-6, 91–92 | 65.41 | 60.23 |
| 8H-1, 67–68 | 67.17 | 86.38 |
| 8H-2, 119–120 | 69.19 | 55.40 |
| 8H-3, 67–68 | 70.17 | 86.22 |
| 8H-4, 11–12 | 71.11 | 61.57 |
| 8H-4, 15–16 | 71.15 | 34.81 |
| 8H-5, 66–67 | 73.16 | 77.03 |
| 8H-6, 66–67 | 74.66 | 84.57 |
| 9H-1, 93–94 | 76.93 | 62.79 |
| 9H-2, 76–77 | 78.26 | 77.32 |
| 9H-2, 86–87 | 78.36 | 64.83 |
| 9H-4, 64–65 | 81.14 | 87.70 |
| 9H-5, 140–141 | 83.40 | 60.87 |
| 10H-1, 53–54 | 86.03 | 67.16 |
| 10H-2, 144–145 | 88.44 | 37.46 |
| 10H-3, 71–72 | 89.21 | 93.49 |
| 10H-4, 95–96 | 90.95 | 80.78 |
| 10H-5, 24–25 | 91.74 | 88.28 |
| 10H-6, 56–57 | 93.56 | 73.62 |
| 11H-1, 89–90 | 95.89 | 87.73 |
| 11H-3, 89–90 | 98.89 | 61.17 |
| 11H-3, 101–102 | 99.01 | 86.07 |
| 11H-3, 117–118 | 99.17 | 52.67 |
| 11H-3, 131–132 | 99.31 | 88.47 |
| 11H-5, 91–92 | 101.91 | 69.83 |
| 11H-5, 101–102 | 102.01 | 89.86 |
| 11H-6, 28–29 | 102.78 | 88.05 |
| 12H-1, 98–99 | 105.48 | 63.23 |
| 12H-1, 120–121 | 105.70 | 83.19 |
| 12H-3, 19–20 | 107.69 | 83.76 |
| 12H-3, 55–56 | 108.05 | 58.34 |
| 12H-3, 71–72 | 108.21 | 80.75 |
| 12H-4, 130–131 | 110.30 | 63.43 |
| 12H-5, 63–64 | 111.13 | 76.23 |
| 12H-5, 90–91 | 111.40 | 78.23 |
| 12H-6, 94–95 | 112.94 | 81.82 |
| 13H-1, 86–87 | 114.86 | 86.48 |
| 13H-2, 60–61 | 116.10 | 83.19 |
| 13H-2, 85–86 | 116.35 | 54.12 |
| 13H-2, 100–101 | 116.50 | 78.11 |
| 13H-3, 39–40 | 117.39 | 67.67 |
| 13H-3, 53–54 | 117.53 | 79.51 |
| 13H-5, 25–26 | 120.25 | 46.32 |
| 13H-6, 120–121 | 122.70 | 62.61 |
| 14H-1, 69–70 | 124.19 | 76.83 |
| 14H-2, 60–61 | 125.60 | 90.44 |
| 14H-2, 89–90 | 125.89 | 70.75 |
| 14H-4, 12–13 | 128.12 | 62.15 |
| 14H-4, 34–35 | 128.34 | 81.41 |
| 14H-4, 78–79 | 128.78 | 85.85 |
| 14H-6, 87–88 | 131.87 | 94.81 |
| 159-958B- | | |
| 1H-1, 39–40 | 0.39 | 70.94 |
| 1H-2, 39–40 | 1.89 | 68.01 |
| 1H-2, 80–81 | 2.30 | 66.94 |
| 1H-3, 39–40 | 3.39 | 59.66 |
| 1H-4, 30–31 | 4.80 | 53.41 |
| 1H-5, 81–82 | 6.81 | 76.05 |

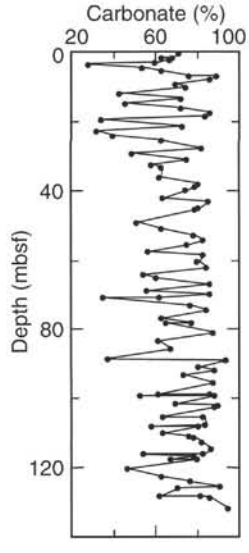


Figure 9. Carbonate percentage vs. depth in Holes 958A and 958B.

trate, in Figure 10, the data from the top of Site 958 using an arbitrary 10-m offset for Core 159-958A-1H. In the following descriptions and discussion we refer to the official "mbsf" values for Hole 958A even though the actual mbsf values are approximately 7–10 m deeper. This way, we ensure compatibility with the other data reported in this chapter.

## Physical Properties Units

### *Description*

Cores 159-958A-1H through 14H were measured on board for gamma-ray attenuation (GRAPE) density, natural gamma radiation, magnetic susceptibility and *P*-wave velocity. No further measurements were conducted on the ship, and the cores were shipped to ODP/TAMU in College Station, TX.

Sampling for discrete physical properties measurements was done during the June 1995 description and sampling meeting. A shipboard-equivalent pycnometer and other equipment for gravimetric density determination were available at ODP/TAMU. We took 20-$cm^3$ samples and determined the wet and dry mass to calculate water content. A freeze-drier was used instead of a convection oven to make the dried samples available later for grain size and other analyses. Dry volumes of subsamples of 6–9 g were determined with the gas pycnometer. Because of the slightly different procedure and laboratory environment on shore, we could not use the IP/4D program

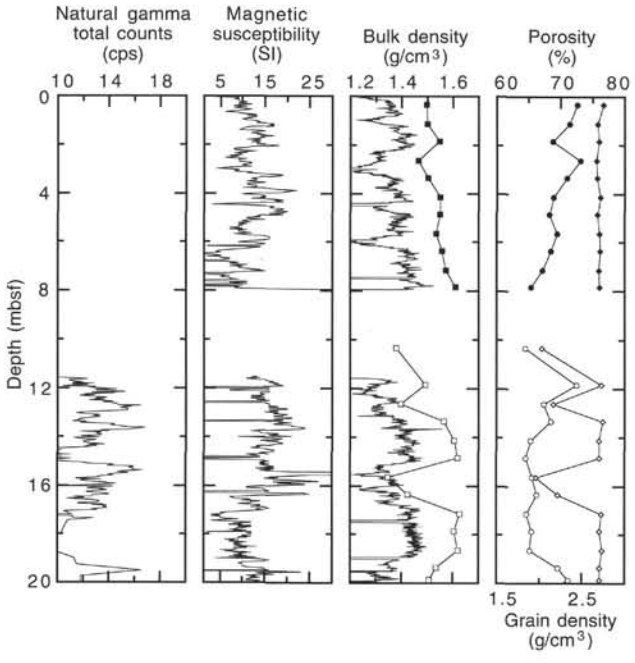


Figure 10. Uppermost recovered section of Hole 958A (top part of figures) and Core 159-958B-1H data (bottom part of figures). The Hole 958A data, which lack a mud-line determination, are arbitrarily offset from "mbsf" depth by 10 m (see text). Note that the top records of the two holes cannot be correlated (i.e., there is a coring gap of unknown lengths). Diamonds = grain densities, circles = porosities, squares = bulk densities determined by the gravimetric method. Solid symbols = Core 159-958B-1H data, open symbols = Hole 958A data. Natural gamma radiation apparently was not measured on Core 159-958B-1H.

used on the ship for moisture-density calculations. Grain densities were calculated directly from dry masses and volumes, while bulk densities were calculated using the water content determined from the main sample. Salt corrections were applied appropriately (Table 5).

The results show that gravimetric densities are higher than GRAPE by about 0.15 to 0.2 g/cm$^3$, or approximately 10%, whereas the relative trends are very similar (Figs. 10, 11). This difference can be explained by changes made to the GRAPE system (hardware or software) on one of the recent legs.

Based on the core physical properties, the sediment section recovered at Site 958 can be divided into five characteristic units (Fig. 11). Unit P-1 (0–28.0 mbsf) shows the largest variations in porosity and natural gamma radiation. Grain density varies strongly in the upper part (0–8 mbsf), and porosity shows the most extreme fluctuation in the middle part of the unit (8–22 mbsf). Grain density has a mean of 2.63 g/cm$^3$ and a relatively large standard deviation of 0.20 g/cm$^3$ due to the low values in the upper part of the unit. Fluctuations in bulk density are mostly due to variations in porosity. Magnetic susceptibility is relatively high at more than 10 SI units, and natural gamma radioactivity fluctuates between the lowest (10 cps) and highest (17 cps) values measured at Site 958.

Unit P-2 (28.0–45.0 mbsf) is the most anomalous interval in Hole 958A. Porosity continues its steady decrease and shows less variability downhole from Unit P-1, but grain density and bulk density are sharply offset from the adjacent values. The low and constant grain density (mean 2.15 g/cm$^3$; standard deviation 0.04 g/cm$^3$) and lack of offset in porosity indicate a drastic change in lithology. This is also reflected in the flat magnetic susceptibility curve at low values of about 5 SI units (Fig. 11). Natural gamma radiation, however, still remains relatively high in this interval. No anomaly in uranium, thorium, or potassium content is observed.

In Unit P-3 (45.0–91.5 mbsf), grain density returns to a high mean value of 2.70 g/cm$^3$ with a low standard deviation of 0.03 g/cm$^3$. Porosity and bulk density resume their linear increase from values in Unit P-1, and porosity continues to decrease linearly. Bulk density, magnetic susceptibility, and natural gamma radiation show cyclic variations. The unit is divided in two subunits based on a sharp decrease in natural gamma radiation, which to a lesser degree occurs with all other properties as well. The bottom of Unit P-3 shows a sharp offset in all properties except grain density. The increase in bulk density is mirrored and directly related to a decrease in porosity.

Unit P-4 (91.5–120.0 mbsf) properties show similar trends as in Unit P-3. Porosity and densities are also very similar in range. Grain density is constant with a mean of 2.71 g/cm$^3$ and a standard deviation of 0.08. Porosity decreases steadily, whereas bulk density increases. The transition to Unit P-5 is characterized by a sharp change in gradient of porosity and drop in magnetic susceptibility and bulk density. Unit P-5 shows high scatter in grain and bulk density, high grain densities (mean: 3.21 g/cm$^3$; standard deviation 0.56 g/cm$^3$), and an anomalous porosity trend.

### *Discussion*

The bulk of the Site 958 sediment section has a constant grain density of about 2.7 g/cm$^3$, which is in excellent agreement with the high carbonate content of these sediments (see "Lithostratigraphy" section, this chapter). Unit P-2 is an exception with a rather low grain density of 2.15 g/cm$^3$. This, and the disappearance of the magnetic susceptibility signal, indicate a significantly different sediment composition in Unit P-2. The upper boundary of Unit P-2 corresponds reasonably well with the change from lithologic Subunit IA to IB (see "Lithostratigraphy" section, this chapter), and a change in sedimentation rate (see "Biostratigraphy" section, this chapter). Smear-slide analysis indicates an interval of somewhat higher quartz and biosilica content within Unit P-2, which may, in part, explain the lower grain densities. However, further sedimentologic analysis is needed to resolve this. The lower boundary of Unit P-2 correlates with a possible hiatus (see "Biostratigraphy" section, this chapter).

The sharp offset in all physical properties at 91.5 m suggests either a major paleoceanographic change or an erosional unconformity. The physical character could be indicative of a cemented horizon that prevents pore-water diffusion upsection. Indeed, a hiatus may be interpreted at this level from the tentative sedimentation rate curve (see "Biostratigraphy" section, this chapter). The sediments correlative with Unit P-4 show a distinct, light-gray, clayey layering not observed in higher units (see "Lithostratigraphy" section, this chapter).

Finally, another significant boundary has been penetrated at 120 m. Grain density values as well as the porosity trend are anomalous in Unit P-5. Olive gray, fining-upward layers were observed in this unit as well as in Unit P-1 (see "Lithostratigraphy" section, this chapter). They are tentatively interpreted as organic-rich turbidites and are probably the cause of relatively high scatter in physical properties in these intervals.

## REFERENCES

Cande, S.C., and Kent, D.V., 1992. A new geomagnetic polarity time scale for the Late Cretaceous and Cenozoic. *J. Geophys. Res.*, 97:13917–13951.

deMenocal, P., Bloemendal, J., and King, J., 1991. A rock-magnetic record of monsoonal dust deposition to the Arabian Sea: evidence for a shift in the mode of deposition at 2.4 Ma. *In* Prell, W.L., Niitsuma, N., et al., *Proc. ODP, Sci. Results,* 117: College Station, TX (Ocean Drilling Program), 389–407.

Kirschvink, J.L., 1980. The least-squares line and plane and the analysis of palaeomagnetic data. *Geophys. J. R. Astron. Soc.*, 62:699–718.

Martini, E., and Müller, C., 1986. Current Tertiary and Quaternary calcareous nannoplankton stratigraphy and correlations. *Newsl. Stratigr.*, 16:99–112.

Munsell Soil Color Charts, 1971. Baltimore (Munsell Color).

Ruddiman, W., Sarnthein, M., Baldauf, J., et al., 1988. *Proc. ODP, Init. Repts.*, 108 (Sections 1 and 2): College Station, TX (Ocean Drilling Program).

Srivastava, S.P., Arthur, M., Clement, B., et al., 1987. *Proc. ODP, Init. Repts.*, 105: College Station, TX (Ocean Drilling Program).

Weaver, P.P.E., Schmincke, H.-U., Firth, J.V., et al., in press. *Proc. ODP, Init. Repts.*, 157: College Station, TX (Ocean Drilling Program).

Young, J.R., 1991. A Quaternary nannofossil range chart. *INA Newsl.*, 13:14–17.

**Ms 159TIR-001**

**Table 5. Index properties from Holes 958A and 958B.**

| Core, section, interval (cm) | Bulk density (g/cm$^3$) | Grain density (g/cm$^3$) | Porosity (%) |
|---|---|---|---|
| 159-958A- | | | |
| 1H-1, 33–38 | 1.381 | 2.030 | 64.5 |
| 1H-2, 33–38 | 1.494 | 2.731 | 72.5 |
| 1H-2, 113–118 | 1.398 | 2.170 | 67.4 |
| 1H-3, 33–38 | 1.566 | 2.748 | 68.5 |
| 1H-3, 113–118 | 1.605 | 2.699 | 65.3 |
| 1H-4, 33–38 | 1.621 | 2.708 | 64.6 |
| 1H-4, 113–118 | 1.348 | 1.965 | 65.6 |
| 1H-5, 33–38 | 1.426 | 2.219 | 66.3 |
| 1H-5, 113–118 | 1.627 | 2.730 | 64.7 |
| 1H-6, 33–38 | 1.605 | 2.709 | 65.5 |
| 1H-6, 113–118 | 1.621 | 2.740 | 65.2 |
| 1H-7, 33–38 | 1.536 | 2.707 | 69.6 |
| 2H-1, 33–38 | 1.509 | 2.710 | 71.2 |
| 2H-1, 113–118 | 1.611 | 2.690 | 64.8 |
| 2H-2, 33–38 | 1.440 | 2.643 | 74.3 |
| 2H-2, 113–118 | 1.525 | 2.700 | 70.1 |
| 2H-3, 33–38 | 1.415 | 2.635 | 75.7 |
| 2H-3, 113–118 | 1.574 | 2.706 | 67.3 |
| 2H-4, 33–38 | 1.599 | 2.697 | 65.7 |
| 2H-5, 33–38 | 1.474 | 2.659 | 72.5 |
| 2H-4, 113–118 | 1.436 | 2.649 | 74.7 |
| 2H-5, 113–118 | 1.580 | 2.690 | 66.6 |
| 2H-6, 33–38 | 1.616 | 2.764 | 66.0 |
| 2H-6, 113–118 | 1.561 | 2.710 | 68.1 |
| 2H-7, 33–38 | 1.580 | 2.717 | 67.2 |
| 3H-1, 33–38 | 1.521 | 2.674 | 69.9 |
| 3H-1, 113–118 | 1.619 | 2.695 | 64.4 |
| 3H-2, 33–38 | 1.588 | 2.700 | 66.4 |
| 3H-2, 113–118 | 1.465 | 2.641 | 72.7 |
| 3H-3, 33–38 | 1.616 | 2.710 | 64.9 |
| 3H-3, 113–118 | 1.629 | 2.657 | 63.0 |
| 3H-4, 33–38 | 1.607 | 2.702 | 65.3 |
| 3H-4, 113–118 | 1.564 | 2.680 | 67.4 |
| 3H-5, 33–38 | 1.569 | 2.718 | 67.8 |
| 3H-5, 113–118 | 1.614 | 2.710 | 65.0 |
| 3H-6, 33–38 | 1.571 | 2.721 | 67.8 |
| 3H-6, 113–118 | 1.610 | 2.731 | 65.7 |
| 4H-1, 33–38 | 1.453 | 2.201 | 63.5 |
| 4H-1, 113–118 | 1.460 | 2.203 | 63.0 |
| 4H-2, 33–38 | 1.446 | 2.180 | 63.5 |
| 4H-2, 113–118 | 1.462 | 2.175 | 62.0 |
| 4H-3, 33–38 | 1.466 | 2.210 | 62.7 |
| 4H-3, 113–118 | 1.470 | 2.181 | 61.5 |
| 4H-4, 33–38 | 1.473 | 2.184 | 61.3 |
| 4H-4, 113–118 | 1.479 | 2.134 | 59.0 |
| 4H-5, 33–38 | 1.449 | 2.143 | 62.1 |
| 4H-5, 113–118 | 1.517 | 2.194 | 57.9 |
| 4H-6, 33–38 | 1.433 | 2.112 | 62.4 |
| 4H-6, 113–118 | 1.466 | 2.177 | 61.7 |
| 4H-7, 33–38 | 1.487 | 2.154 | 59.0 |
| 5H-1, 33–38 | 1.417 | 2.099 | 63.5 |
| 5H-1, 113–118 | 1.467 | 2.113 | 59.3 |
| 5H-2, 33–38 | 1.484 | 2.084 | 56.6 |
| 5H-2, 113–118 | 1.438 | 2.093 | 61.2 |
| 5H-3, 33–38 | 1.471 | 2.123 | 59.3 |
| 5H-3, 113–118 | 1.475 | 2.132 | 59.3 |
| 5H-4, 33–38 | 1.509 | 2.200 | 58.8 |
| 5H-4, 113–118 | 1.482 | 2.134 | 58.7 |
| 5H-5, 33–38 | 1.485 | 2.154 | 59.2 |
| 5H-5, 113–118 | 1.649 | 2.689 | 62.5 |
| 5H-6, 33–38 | 1.654 | 2.718 | 62.8 |
| 5H-6, 113–118 | 1.649 | 2.663 | 61.9 |
| 6H-1, 33–38 | 1.633 | 2.712 | 63.9 |
| 6H-1, 113–118 | 1.640 | 2.715 | 63.6 |
| 6H-2, 33–38 | 1.630 | 2.681 | 63.5 |
| 6H-2, 113–118 | 1.669 | 2.706 | 61.6 |
| 6H-3, 33–38 | 1.706 | 2.686 | 58.9 |
| 6H-3, 113–118 | 1.672 | 2.694 | 61.2 |
| 6H-4, 33–38 | 1.717 | 2.646 | 57.3 |
| 6H-4, 113–118 | 1.670 | 2.700 | 61.4 |
| 6H-5, 33–38 | 1.693 | 2.743 | 61.1 |
| 6H-5, 113–118 | 1.682 | 2.685 | 60.4 |
| 6H-6, 33–38 | 1.673 | 2.710 | 61.5 |
| 6H-6, 113–118 | 1.703 | 2.694 | 59.4 |
| 7H-1, 33–38 | 1.674 | 2.717 | 61.6 |
| 7H-1, 113–118 | 1.671 | 2.708 | 61.6 |
| 7H-2, 33–38 | 1.715 | 2.705 | 58.9 |
| 7H-2, 113–118 | 1.700 | 2.720 | 60.1 |
| 7H-3, 33–38 | 1.725 | 2.654 | 57.0 |
| 7H-3, 113–118 | 1.706 | 2.711 | 59.6 |
| 7H-4, 33–38 | 1.693 | 2.697 | 60.0 |
| 7H-4, 113–118 | 1.705 | 2.695 | 59.2 |
| 7H-5, 33–38 | 1.703 | 2.713 | 59.8 |
| 7H-5, 113–118 | 1.684 | 2.727 | 61.2 |
| 7H-6, 33–38 | 1.700 | 2.681 | 59.2 |
| 7H-6, 113–118 | 1.736 | 2.721 | 58.1 |
| 8H-1, 33–38 | 1.698 | 2.674 | 59.1 |
| 8H-1, 113–118 | 1.667 | 2.712 | 61.9 |
| 8H-2, 33–38 | 1.684 | 2.710 | 60.8 |
| 8H-2, 113–118 | 1.674 | 2.660 | 60.3 |
| 8H-3, 33–38 | 1.728 | 2.723 | 58.6 |
| 8H-3, 113–118 | 1.722 | 2.686 | 58.0 |
| 8H-4, 33–38 | 1.704 | 2.719 | 59.9 |
| 8H-4, 113–118 | 1.732 | 2.686 | 57.4 |
| 8H-5, 33–38 | 1.731 | 2.723 | 58.4 |
| 8H-5, 113–118 | 1.716 | 2.690 | 58.4 |
| 8H-6, 33–38 | 1.720 | 2.767 | 60.1 |
| 8H-6, 113–118 | 1.695 | 2.650 | 58.7 |
| 9H-1, 33–38 | 1.734 | 2.679 | 57.1 |
| 9H-1, 113–118 | 1.718 | 2.682 | 58.1 |
| 9H-2, 33–38 | 1.730 | 2.720 | 58.4 |
| 9H-2, 113–118 | 1.719 | 2.700 | 58.6 |
| 9H-3, 33–38 | 1.718 | 2.722 | 59.1 |
| 9H-4, 33–38 | 1.706 | 2.707 | 59.5 |
| 9H-4, 113–118 | 1.722 | 2.669 | 57.5 |
| 9H-5, 33–38 | 1.707 | 2.725 | 59.8 |
| 9H-5, 113–118 | 1.689 | 2.679 | 59.8 |
| 9H-6, 33–38 | 1.730 | 2.704 | 58.0 |
| 9H-6, 113–118 | 1.753 | 2.692 | 56.3 |
| 10H-1, 33–38 | 1.724 | 2.717 | 58.6 |
| 10H-1, 113–118 | 1.747 | 2.681 | 56.3 |
| 10H-2, 33–38 | 1.763 | 2.641 | 54.3 |
| 10H-2, 113–118 | 1.769 | 2.706 | 55.7 |
| 10H-3, 33–38 | 1.841 | 2.741 | 52.4 |
| 10H-3, 113–118 | 1.829 | 2.674 | 51.2 |
| 10H-4, 33–38 | 1.854 | 2.791 | 53.0 |
| 10H-4, 113–118 | 1.824 | 2.744 | 53.5 |
| 10H-5, 33–38 | 1.706 | 2.723 | 59.8 |
| 10H-5, 113–118 | 1.677 | 2.733 | 61.8 |
| 10H-6, 33–38 | 1.685 | 2.717 | 61.0 |
| 10H-6, 113–118 | 1.675 | 2.750 | 62.3 |
| 10H-7, 33–38 | 1.719 | 2.735 | 59.4 |
| 11H-1, 33–38 | 1.670 | 2.745 | 62.5 |
| 11H-1, 113–118 | 1.720 | 2.751 | 59.7 |
| 11H-2, 33–38 | 1.736 | 2.761 | 59.0 |
| 11H-2, 113–118 | 1.707 | 2.734 | 60.1 |
| 11H-3, 33–38 | 1.716 | 2.761 | 60.2 |
| 11H-3, 113–118 | 1.740 | 2.649 | 56.0 |
| 11H-4, 33–38 | 1.703 | 2.733 | 60.3 |
| 11H-4, 113–118 | 1.725 | 2.734 | 59.0 |
| 11H-5, 33–38 | 1.722 | 2.745 | 59.4 |
| 11H-5, 113–118 | 1.716 | 2.699 | 58.7 |
| 11H-6, 33–38 | 1.727 | 2.689 | 57.8 |
| 11H-6, 113–118 | 1.718 | 2.752 | 59.8 |
| 11H-7, 33–38 | 1.617 | 2.275 | 52.6 |
| 12H-1, 33–38 | 1.758 | 2.717 | 56.6 |
| 12H-1, 113–118 | 1.756 | 2.725 | 57.0 |
| 12H-2, 33–38 | 1.746 | 2.728 | 57.6 |
| 12H-2, 113–118 | 1.748 | 2.726 | 57.5 |
| 12H-3, 33–38 | 1.727 | 2.721 | 58.6 |
| 12H-3, 113–118 | 1.778 | 2.710 | 55.2 |
| 12H-4, 33–38 | 1.757 | 2.744 | 57.4 |
| 12H-4, 113–118 | 1.791 | 2.706 | 54.4 |
| 12H-5, 33–38 | 1.730 | 2.705 | 58.0 |
| 12H-5, 113–118 | 1.770 | 2.737 | 56.5 |
| 12H-6, 33–38 | 1.762 | 2.706 | 56.1 |
| 12H-6, 113–118 | 1.777 | 2.725 | 55.7 |

**Table 5 (continued).**

| Core, section, interval (cm) | Bulk density (g/cm$^3$) | Grain density (g/cm$^3$) | Porosity (%) |
|---|---|---|---|
| 13H-1, 33–38 | 1.783 | 2.705 | 54.8 |
| 13H-1, 113–118 | 1.812 | 2.662 | 51.9 |
| 13H-2, 33–38 | 1.792 | 2.712 | 54.5 |
| 13H-2, 113–118 | 1.802 | 2.705 | 53.7 |
| 13H-3, 33–38 | 1.774 | 2.675 | 54.6 |
| 13H-3, 113–118 | 1.800 | 2.667 | 52.8 |
| 13H-4, 33–38 | 1.795 | 2.659 | 52.8 |
| 13H-4, 113–118 | 1.809 | 2.688 | 52.8 |
| 13H-5, 33–38 | 1.937 | 2.993 | 53.6 |
| 13H-5, 113–118 | 2.189 | 4.138 | 62.6 |
| 13H-6, 33–38 | 2.138 | 4.008 | 62.7 |
| 13H-7, 33–38 | 2.017 | 3.614 | 61.7 |
| 13H-6, 113–118 | 1.819 | 2.651 | 51.2 |
| 14H-1, 33–38 | 1.842 | 2.813 | 54.3 |
| 14H-1, 113–118 | 1.673 | 2.629 | 59.6 |
| 14H-2, 33–38 | 1.681 | 2.502 | 55.5 |
| 14H-2, 113–118 | 1.729 | 2.871 | 61.8 |
| 14H-3, 33–38 | 1.954 | 3.822 | 66.8 |
| 14H-3, 113–118 | 2.007 | 3.751 | 63.9 |
| 14H-4, 33–38 | 1.745 | 2.690 | 56.7 |
| 14H-4, 113–118 | 1.675 | 2.482 | 55.4 |
| 14H-5, 33–38 | 1.767 | 3.084 | 63.9 |
| 14H-5, 113–118 | 1.907 | 3.474 | 64.0 |
| 14H-6, 33–38 | 1.813 | 3.212 | 63.9 |
| 14H-6, 113–118 | 1.969 | 3.788 | 65.8 |
| 159-958B- | | | |
| 1H-1, 33–38 | 1.497 | 2.751 | 72.6 |
| 1H-1, 113–118 | 1.500 | 2.685 | 71.4 |
| 1H-2, 33–38 | 1.547 | 2.702 | 68.8 |
| 1H-2, 113–118 | 1.466 | 2.670 | 73.1 |
| 1H-3, 33–38 | 1.502 | 2.675 | 71.0 |
| 1H-3, 113–118 | 1.550 | 2.715 | 68.9 |
| 1H-4, 33–38 | 1.550 | 2.684 | 68.3 |
| 1H-4, 113–118 | 1.536 | 2.706 | 69.5 |
| 1H-5, 33–38 | 1.558 | 2.718 | 68.5 |
| 1H-5, 113–118 | 1.574 | 2.701 | 67.2 |
| 1H-6, 33–38 | 1.609 | 2.712 | 65.4 |

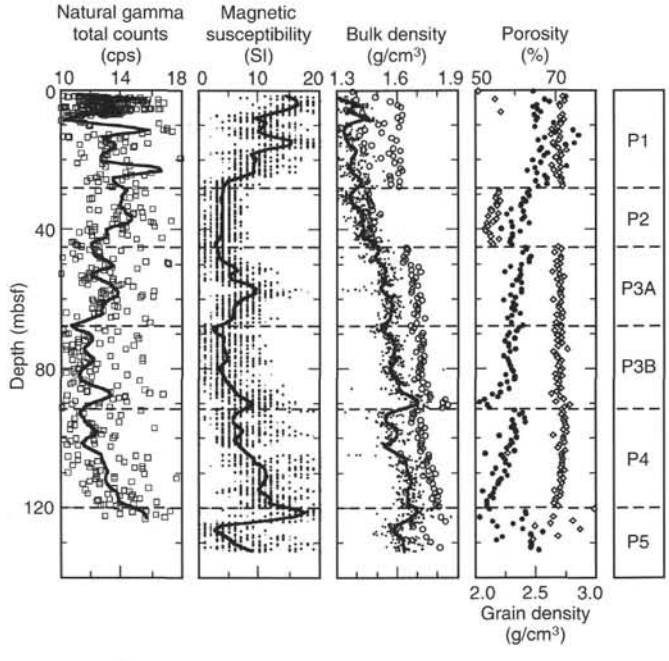


Figure 11. Hole 958A physical properties data and units. Hole 958A data lack a mud-line determination; true depths below seafloor are approximately 9 ± 2 m deeper than official "mbsf" depth. Diamonds = grain densities, solid circles = porosities, open circles = bulk densities determined by the gravimetric method. Thick lines are locally weighted least-square fits (3% of population) of data plotted as small points or squares.